

**Unconventional time-bandwidth performance of resonant cavities with nonreciprocal coupling**Ivan Cardea <sup>1</sup>, Davide Grassani <sup>2</sup>, Jeremy Upham,<sup>3</sup> Sebastian A. Schulz <sup>4</sup>,  
Kosmas L. Tsakmakidis,<sup>5</sup> and Camille-Sophie Brès<sup>1,\*</sup><sup>1</sup>*Ecole Polytechnique Fédérale de Lausanne (EPFL), Photonic Systems Laboratory (PHOSL), Lausanne CH-1015, Switzerland*<sup>2</sup>*Dipartimento di Fisica, Università degli Studi di Pavia, via Bassi 6, 27100 Pavia, Italy*<sup>3</sup>*Department of Physics, University of Ottawa, Ottawa, Ontario, Canada*<sup>4</sup>*School of Physics and Astronomy, SUPA, University of St Andrews, St Andrews, KY169SS, United Kingdom*<sup>5</sup>*Section of Condensed Matter Physics, Department of Physics, National and Kapodistrian University of Athens, Panepistimioupolis, GR-157 84, Athens, Greece*

(Received 8 June 2020; revised 5 November 2020; accepted 14 December 2020; published 12 January 2021)

The time-bandwidth limit is a mathematical tenet that affects all reciprocal resonators, stating that the product of the spectral bandwidth that can couple into a resonant system and its characteristic energy decay time is always equal to 1. Here, we develop an analytical and numerical model to show that introducing nonreciprocal coupling to a generalized resonator changes the power balance between the reflected and intracavity fields, which consequently overcomes the time-bandwidth limit of the resonant system. By performing a full evaluation of the time-bandwidth product (TBP) of the modeled resonator, we show that it represents a measure of the increased delay imparted to a light wave, with respect to what the bandwidth of the reciprocal resonant structure would allow to the same amount of in-coupled power. No longer restricted to the value 1, we show that the TBP can instead be used as a figure of merit of the improvement in intracavity power enhancement due to the nonreciprocal coupling.

DOI: [10.1103/PhysRevA.103.013716](https://doi.org/10.1103/PhysRevA.103.013716)**I. INTRODUCTION**

The capability to slow down or trap light without imposing an excessive distortion to the signal is a key tool of many research areas such as optical communications [1,2], quantum information processing [3], metamaterials [4], and photovoltaics [5–7]. In particular, it is of fundamental importance in all the applications requiring optical signal processing or light storage [8–14]. Thus far, owing to the progress attained in the development of slow light devices, new frontiers of light propagation have been achieved, in which light can be dramatically slowed [15], captured and then released at a later time [16–18], or even stopped altogether [19–21]. Generally, what is required from the practical point of view is the ability to impart a delay to a signal that is independent of the signal's bandwidth. For instance, in wavelength division multiplexed (WDM) multichannel systems, storage devices and delay lines are used at the receiver end to store high-rate data packets as they are read out at a slower rate or for queuing while the transmitter awaits access to the network [22,23].

In the last two decades, different implementations of resonant structures have been explored for the realization of delay lines and storage devices [24–31], since they offer a long effective delay at small footprints. Resonant cavities are also widely used in nonlinear optics applications, such as frequency comb and Kerr soliton generation [32,33], where the intracavity power enhancement helps to reduce the input power required to induce nonlinear effects. As is well

known, reducing the cavity bandwidth is a way to increase the interaction time, as well as the power enhancement factor. However, this leads to a constraint that unavoidably imposes a trade-off between the delay time achievable and the width of the operational spectral bandwidth [34–36]. In mathematical terms, this trade-off is described by the time-bandwidth limit, a fundamental rule that arises from Fourier-reciprocity considerations, which dictates that the time-bandwidth product (TBP) must be  $\Delta\omega\tau = 1$ , with  $\Delta\omega$  the system bandwidth and  $\tau$  the energy decay time [37–39]. Both high finesse and losses limit the storage capacity of microresonator-based devices [40]. Precisely the same issue limits slow light devices, which are equivalently limited by large group velocity dispersion and losses [8,41].

Recently, a proposal [42] indicated that breaking Lorentz reciprocity can overcome the time-bandwidth limit in a resonant system. Following this idea, we have experimentally demonstrated [43] a fully nonreciprocal cavity with TBP exceeding the “fundamental” limit by a factor of 30 and limited only by intrinsic losses. We also proposed that the concept of the bandwidth that the resonator can “accept” (the *acceptance bandwidth*  $\Delta\omega_{\text{acc}}$ ) can be different from what is considered the *cavity bandwidth*  $\Delta\omega_{\text{cav}}$ , which is simply the inverse of the characteristic decay time ( $\tau$ ).

Here, we present a generalized theoretical model of a resonant cavity having a nonreciprocal coupling element. We analytically derive the frequency response of the reflected and intracavity fields, their associated powers, and the TBP of the system as a function of the degree of nonreciprocity, i.e., the difference between the in-coupling and out-coupling energy rate. We numerically validate this model simulating

\*camille.bres@epfl.ch

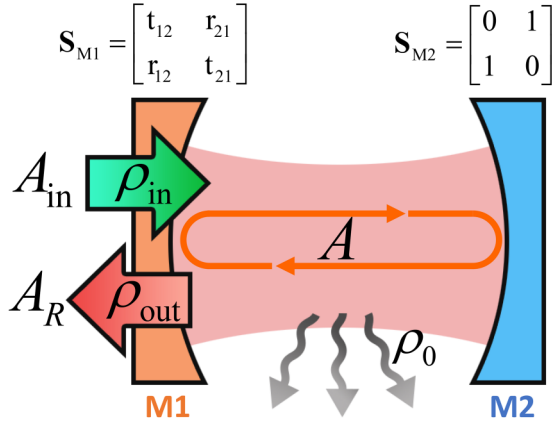


FIG. 1. Layout of a Gires-Tournois resonator with a nonreciprocal front mirror, whose transmission coefficients depend on the direction of wave propagation, and a fully reflective rear mirror.

a cavity where nonreciprocity is obtained by breaking its time invariance [44], as it provides a direct way to implement this device using off-the-shelf telecom components [43]. Our results show that resonant systems with a nonreciprocal coupling can provide a longer delay or storage time and a significant improvement of the intracavity power enhancement, with respect to their reciprocal counterpart, which is strongly desirable in all the applications that demand high efficiency in nonlinear processes. Moreover, we demonstrate that such improvement of intracavity power enhancement is nothing but the TBP of the system, quantitatively linking the degree of nonreciprocity of a resonator to a figure of merit for nonlinear optical processes.

## II. THEORETICAL MODEL

### A. Resonant system with nonreciprocal coupling

To analyze a resonant system with nonreciprocal coupling, we consider a Gires-Tournois resonator [45,46]. The back mirror (M2) is fully reflective, while the front mirror (M1) is characterized by the following generic scattering matrix:

$$\mathbf{S}_{M1} = \begin{bmatrix} \mathbf{t}_{12} & \mathbf{r}_{21} \\ \mathbf{r}_{12} & \mathbf{t}_{21} \end{bmatrix}, \quad (1)$$

where  $\mathbf{t}_{12}$  ( $\mathbf{t}_{21}$ ) and  $\mathbf{r}_{12}$  ( $\mathbf{r}_{21}$ ) are the complex transmission and reflection coefficients, respectively, of a wave incident from outside (inside) the resonator. A schematic illustration of such resonant system is shown in Fig. 1, where  $A$ ,  $A_{in}$ , and  $A_R$  represent the complex amplitudes of the intracavity, and the incoming and the (total) reflected wave, respectively. In this system the front mirror constitutes the only physical port. Therefore, the total in- and out-coupling radiative energy rates,  $\rho_{in}$  and  $\rho_{out}$ , respectively, are given by  $\rho_{in} = |\mathbf{t}_{12}|^2/T_{RT}$  and  $\rho_{out} = |\mathbf{t}_{21}|^2/T_{RT}$ , with  $T_{RT}$  being the cavity round-trip time, while  $\rho_0$  is the intrinsic, or nonradiative, energy decay rate. A nonreciprocal coupling implies that  $\rho_{in}$  and  $\rho_{out}$  are different due to a nonreciprocal transmittance of the front mirror ( $|\mathbf{t}_{12}|^2 \neq |\mathbf{t}_{21}|^2$ ) [43]. Consequently, the difference  $|\mathbf{t}_{12}|^2 - |\mathbf{t}_{21}|^2$  can be seen as a measure of the *degree of nonreciprocity* of the system. Note that the analytical model aims at studying the implication of decoupling input

and output energy rates in a resonant system irrespective to the mechanism used to induce the nonreciprocal coupling, which, in any case, must ensure the conservation of energy [47–50]. In particular, the model does not presume how the scattering matrix with such characteristics is generated; thus the origin of the nonreciprocity (e.g., external magnetic field bias, temporal variance, nonlinearity, etc.) [47,51] does not have any impact on the TBP and the power balance of the system: As long as the system has such scattering matrix, it can exhibit nonreciprocal coupling. In the following sections, we show that temporal variance is one way to reach this state, but other mechanisms, such as external magnetic field bias or nonlinearity, could also lead to the same outcome. Moreover, although, for the sake of simplicity, we are considering a one-port system, the model can be generalized for multipoint systems just by taking into account the in- and out-coupling energy rates of the other ports.

### B. Derivation of the frequency response

To characterize the frequency response of the system, we use the formalism of the coupling of modes in space also known as power coupling theory (PCT) [37,46,52]. While the temporal coupled mode theory (TCMT) [37,53–56] can also be used to describe the spectral distribution of a resonant mode in an optical cavity, even in the context of nonreciprocity [57,58], the equations on which it is based can approximate the spectral response of a resonator only under the assumption of weak coupling. By using the PCT we therefore carry out an analysis unconstrained by coupling strength assumptions and that can also consider multiple resonant mode profiles. Another distinction is that PCT gives the frequency response of the resonator, which has the shape of an Airy function, while the TCMT approximates the resonant system as a Lorentz oscillator characterized by a single longitudinal mode [59].

The spectral distribution of the intracavity ( $A$ ) and reflected ( $A_R$ ) fields can be expressed as follows (details in Appendix A):

$$A(\omega) = \frac{\sqrt{\rho_{in} T_{RT}} \sqrt{a_d}}{1 - \exp[\ln(|\mathbf{r}_{21}|) - (\rho_0/2 + j\Delta\omega)T_{RT}]} A_{in}(\omega), \quad (2)$$

$$A_R(\omega) = \left\{ \mathbf{r}_{12} + \frac{\sqrt{\rho_{in} \rho_{out}} T_{RT} a_d \exp[-j(\Delta\omega T_{RT} - \phi_{21}^r)]}{1 - \exp[\ln(|\mathbf{r}_{21}|) - (\rho_0/2 + j\Delta\omega)T_{RT}]} \right\} A_{in}(\omega), \quad (3)$$

where  $\phi_{21}^r$  is the phase of  $\mathbf{r}_{21}$ ,  $a_d$  is the field inner circulation factor that accounts for the nonradiative loss of the resonator,  $\Delta\omega = \omega - \omega_0$  is the frequency detuning from resonance, and the field of the incident wave  $A_{in}(\omega)$  is assumed to have a flat frequency distribution over one free spectral range (FSR =  $1/T_{RT}$ ).

### C. Analysis of the power balance of the resonant system

To study the effect of nonreciprocity on the power balance of the resonator, we calculate the total reflected and intracavity powers encased in one FSR. When normalized to the input power and the FSR, expressed in angular frequency ( $\Delta\omega_{FSR} = 2\pi/T_{RT}$ ), they are given by the following expressions,

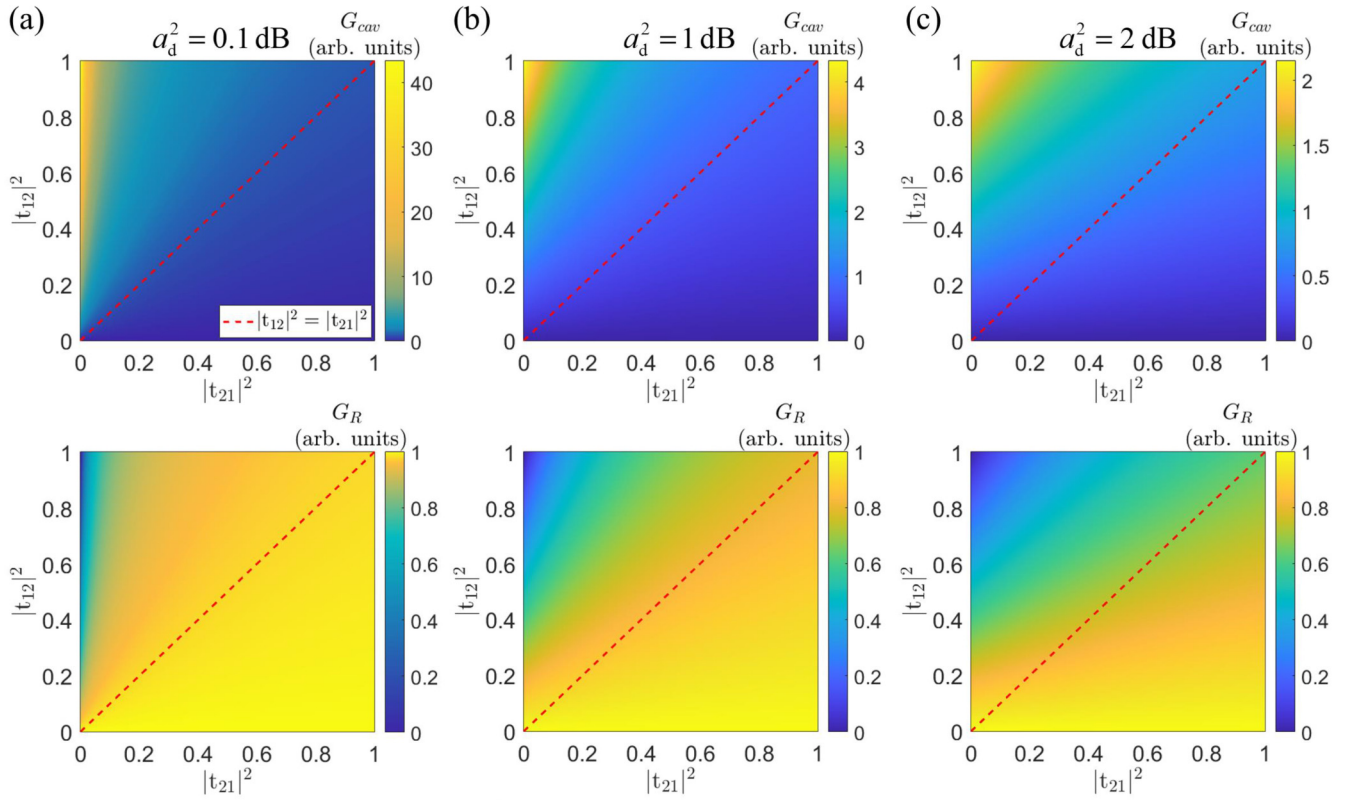


FIG. 2. Graphs in color scale of the total intracavity (top row) and reflected (bottom row) power encased in one FSR, normalized to the total input power and  $\Delta\omega_{\text{FSR}}$ , plotted as a function of the in-coupling and out-coupling transmittances. The values are related to a resonator with (a) 0.1, (b) 1, and (c) 2 dB of internal loss, while the red dashed line indicates the points relative to the reciprocal coupling.

respectively:

$$G_R = \frac{1}{\Delta\omega_{\text{FSR}}} \int_{\text{FSR}} \left| \frac{A_R(\omega)}{A_{\text{in}}(\omega)} \right|^2 d\omega$$

$$G_{\text{cav}} = \frac{1}{\Delta\omega_{\text{FSR}}} \int_{\text{FSR}} \left| \frac{A(\omega)}{A_{\text{in}}(\omega)} \right|^2 d\omega, \quad (4)$$

where the argument of the integral of  $G_{\text{cav}}$  is nothing else but the intracavity power enhancement. Therefore,  $G_{\text{cav}}$  represents the total power enhancement attained over one FSR.

First, we study the problem focusing on a purely theoretical analysis, plotting the values of  $G_{\text{cav}}$  and  $G_R$ , as a function of the in- and out-coupling transmittance. Figure 2(a) shows the case with  $a_d^2 = 0.1$  dB,  $T_{\text{RT}} = 100$  ns, and the phases of  $\mathbf{r}_{12}$  and  $\mathbf{r}_{21}$  both set to 0. The red dashed lines indicate the states where coupling is reciprocal ( $|t_{12}|^2 = |t_{21}|^2$ ). The maximum value of  $G_{\text{cav}}$  occurs when  $|t_{12}|^2 = 1$  and  $|t_{21}|^2 = 0$ , i.e., when there is total inward transmission and zero outward transmission through the front mirror. Conversely, when  $|t_{12}|^2 = 0$ , nothing enters in the resonators and, as expected,  $G_{\text{cav}} = 0$ . More importantly, we note that, owing to the nonreciprocal coupling, the intracavity power can be enhanced by more than a factor of 40 with respect to the reciprocal case (red dashed line). The graph of  $G_R$  shows an inverse behavior, with a peak value occurring at  $|t_{12}|^2 = 0$ , and a minimum when  $|t_{12}|^2 = 1$  and  $|t_{21}|^2 = 0$ . The graphs in Figs. 2(b) and 2(c) are for 1 and 2 dB of internal (round-trip) loss, respectively. We can see that  $G_{\text{cav}}$  decreases with increasing internal loss for all combinations of  $|t_{12}|^2$  and  $|t_{21}|^2$ , while the maximum value of

$G_R$  does not change because, in this case, the contribution of the out-coupled power, that is affected by the internal loss, is missing. We also note that  $G_R$  exhibits smoother variations as a function of  $|t_{21}|^2$  when the contribution of the internal loss increases.

To validate the theoretical analysis, we compare these results with those obtained from simulations based on a full-wave analysis conducted using the software VPIPHOTONICS [60]. Although the model does not depend on the mechanism used to induce the nonreciprocal coupling, we implement the Gires-Tournois resonator in the form of a figure-nine cavity where the nonreciprocal front mirror is simulated by a time-modulated Sagnac interferometer, as it has been proven to be experimentally implemented with standard telecommunication components [43]. Details on the numerical setup used in the simulations can be found in Appendix B. Through this numerical model, we could arbitrarily and independently vary the in- and out-coupling transmission coefficients of the front mirror. However, for the sake of clarity, we analyze the system for two different cases. As the degree of nonreciprocity is equivalent to the minimum distance from the line of reciprocity for any point in the parameter space considered in Fig. 2, in case (A) we evaluate the spectral response of the system for different degrees of nonreciprocity by considering points meeting the conditions  $|t_{12}|^2 + |t_{21}|^2 = 1$  and  $|t_{12}|^2 \geq |t_{21}|^2$ ; in case (B), aiming at investigating on the behavior of the resonator in the situation where the light is totally trapped in the cavity, we perform the analysis for  $|t_{21}|^2 = 0$  while varying  $|t_{12}|^2$ . In both cases  $a_d^2$  and  $T_{\text{RT}}$  are set to 0.1 dB and

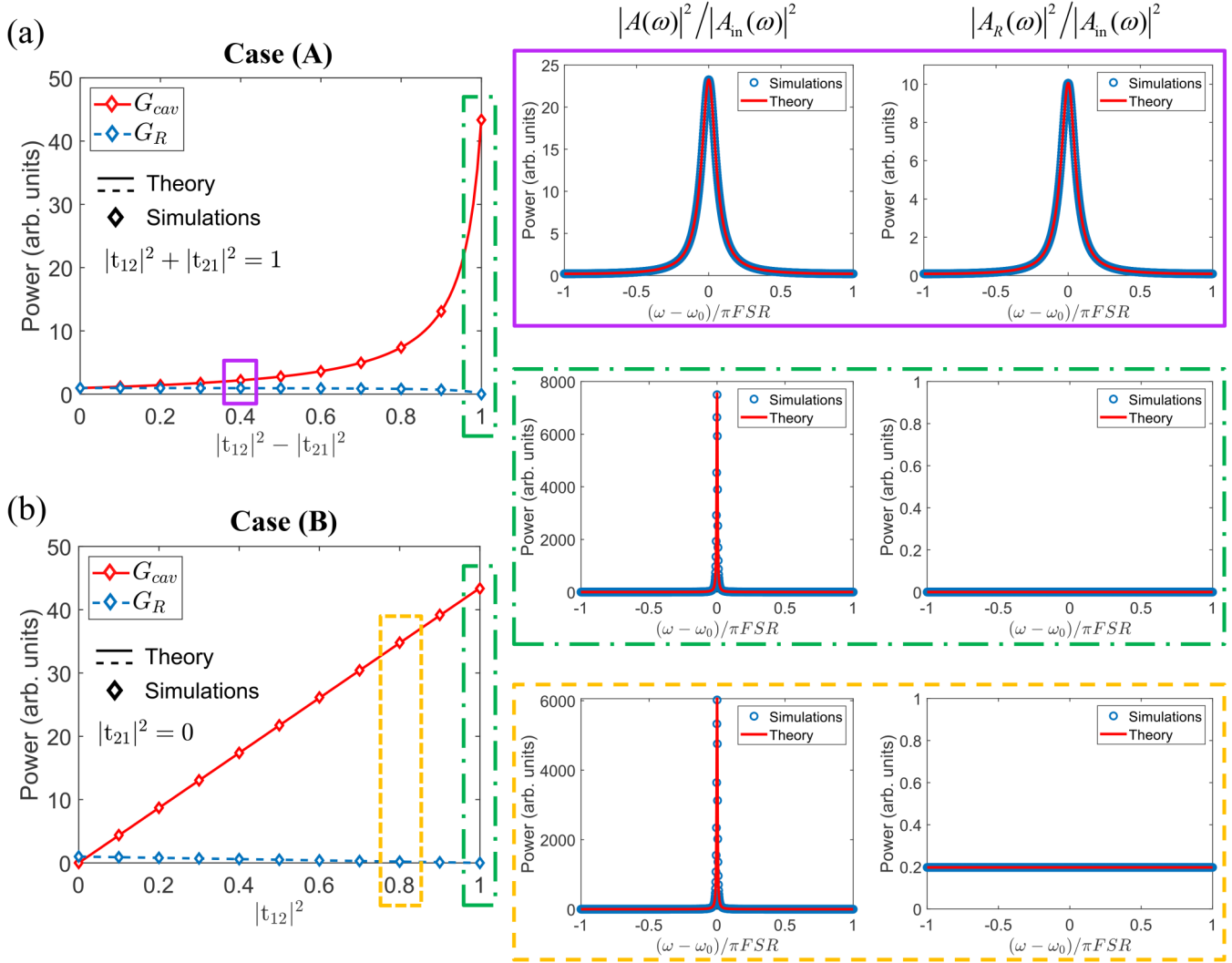


FIG. 3. Left-hand side: comparison of the values obtained from the simulations with those retrieved from Eq. (4) of the total power enhancement and reflected power, encased in one FSR and normalized to it. The graphs are related to the first (a) and the second (b) case of study and plotted as a function of the degree of nonreciprocity and the in-coupling transmittance, respectively. Right-hand side: spectral distribution over one FSR of the reflected power and the intracavity power enhancement. The curves are related to a degree of nonreciprocity equal to 0.4 (violet solid panel) and 1 (green dotted-dashed panel), and to the case with  $|t_{21}|^2 = 0$  and  $|t_{12}|^2 = 0.8$  (yellow dashed panel).

100 ns, respectively, while the phases of  $\mathbf{r}_{12}$  and  $\mathbf{r}_{21}$ , both set to  $\pi/2$ , were retrieved by deriving the equations for the wave interference at the coupling element of the simulating setup [see Eqs. (B5) and (B7) in Appendix B]. The results for case (A) are shown in Fig. 3(a). We can see that  $G_{cav}$  and  $G_R$  have roughly the same value in the reciprocal case, given that the internal loss is small. However, by decoupling  $|t_{12}|^2$  and  $|t_{21}|^2$ ,  $G_{cav}$  exponentially grows with increasing degree of nonreciprocity, taking its maximum value at the highest degree of nonreciprocity, while  $G_R$  decreases. A rather different scenario occurs in case (B), described in Fig. 3(b), where both  $G_{cav}$  and  $G_R$  vary linearly with  $|t_{12}|^2$ . In this case, since  $|t_{21}|^2$  is set to 0,  $G_R$  is a linear function of the reflection coefficient of the front mirror and no cavity resonant mode is coupled out, while the growth of  $G_{cav}$  is due only to the in-coupling energy rate  $\rho_{in}$ , as predicted by Eqs. (2) and (3) respectively. In fact, in the extreme case where also  $|t_{12}|^2 = 0$ , then  $G_{cav} = 0$  and  $G_R$  has a finite value since the incoming power is totally

reflected by the front mirror. The right-hand side of the figure shows the spectral distribution over one FSR of the intracavity power enhancement and the normalized reflected power related to some values of Figs. 3(a) and 3(b). As expected, the bandwidth of the intracavity spectrum, which is given by  $\Delta\omega = (4/T_{RT})\sin^{-1}\{[1 - |\mathbf{r}_{21}|a_d^{-1/2}]/[2(|\mathbf{r}_{21}|a_d^{-1/2})^{-1/2}]\}$ , gets narrower with increasing degree of nonreciprocity since  $|t_{21}|^2$  (which is equal to  $1 - |\mathbf{r}_{21}|^2$ ) decreases. We also note that the zero out-coupling transmission ( $|t_{21}|^2 = 0$ , green dotted-dashed and yellow dashed panel) leads to a reflection spectrum that is no longer dependent on the frequency, since it includes only the contribution of the power reflected by the front mirror. Particularly, in the specific case of fully coupled input power ( $|t_{12}|^2 = 1$ , i.e., maximum degree of nonreciprocity), the reflected power is null, meaning that the light is completely trapped inside the resonator, and dissipated via the internal loss. Importantly, in both cases the numerical results are in good agreement with Eqs. (2)–(4). Therefore,

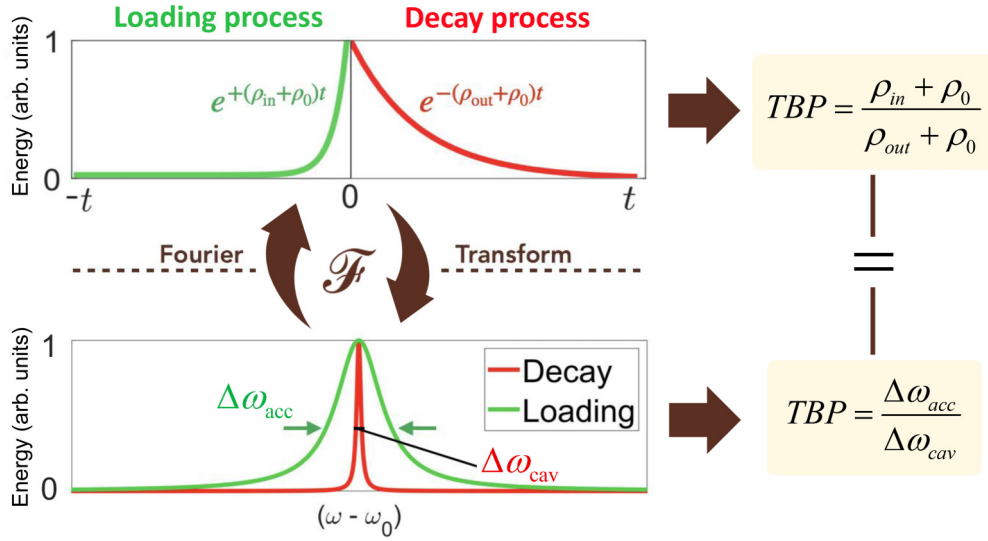


FIG. 4. Derivation of the TBP of a resonant system starting from its loading and decay processes. The TBP is given by the ratio between the acceptance and the cavity bandwidth which are the FWHM of the Lorentzian function associated, through the Fourier transform, to the loading and decay curve, respectively.

the decoupling of the in- and out-coupling energy rates in a resonant system, a consequence of the induced nonreciprocity, can dramatically affect the balance between the reflected and intracavity power and significantly improve the power enhancement provided by the resonator.

### III. EVALUATION OF THE TIME-BANDWIDTH PERFORMANCE

Following the above analysis, we evaluate the TBP for different degrees of nonreciprocity. We recall that the resonator losses, which include both the radiative and nonradiative out-coupling energy rates, are quantified by the linewidth of the Lorentzian profile of the *single* resonant mode and not by the full width at half maximum (FWHM) of the Airy function characteristic of the resonator spectral response [59]. This is a rule that is valid regardless of the strength of the coupling. Therefore, to properly derive the TBP, we use the TCMT to retrieve the Lorentzian mode profile associated to the loading and decay processes of the resonator. As explained in [43], analogously to the decay process of the energy stored in the resonator, which varies in time as  $e^{-(\rho_{out}+\rho_0)t}$ , and sets the bandwidth of the resonator to  $\Delta\omega_{cav} = \rho_{out} + \rho_0$ , we can define a loading process, where the energy builds up in the resonator as  $e^{+(\rho_{in}+\rho_0)t}$  as the time is running backward [53]. Then, the loading rate  $(\rho_{in} + \rho_0)$  represents the acceptance bandwidth of the resonator ( $\Delta\omega_{acc} = \rho_{in} + \rho_0$ ). This concept is illustrated in Fig. 4, where both the loading and decay processes, and their associated bandwidths, are used to calculate the TBP of the system as  $\Delta\omega_{acc}/\Delta\omega_{cav}$  [43].

We calculate the TBP of the resonator in the case of reciprocal and nonreciprocal coupling, and we plot the values in Fig. 5(a) as a function of  $|t_{12}|^2$ . For the nonreciprocal case, we plot three curves corresponding to three values of the absorption loss  $a_d^2$ : 0 (lossless), 0.1, and 0.5 dB, while  $|t_{21}|^2$  is set to 0.1. Owing to the decoupling of the in- and out-coupling energy rates, the TBP linearly increases with the increasing

of  $|t_{12}|^2$  in the case of nonreciprocal coupling, while it is always equal to 1 in the case of reciprocal coupling. A similar scenario (for a time-invariant structure) was introduced in [42].

In Fig. 5(b) the TBP of a resonator with  $a_d^2 = 0.1$  dB is plotted for all the combinations of  $|t_{12}|^2$  and  $|t_{21}|^2$ , with the red dashed line indicating reciprocal coupling ( $|t_{12}|^2 = |t_{21}|^2$ ). The highest TBP occurs at the maximum degree of nonreciprocity, while it becomes smaller than 1 when the degree of nonreciprocity is negative ( $|t_{12}|^2 < |t_{21}|^2$ ).

It is interesting to note that the values of the TBP follow those of  $G_{cav}$  in Fig. 3(a) showing a strict correlation between the TBP and the total power enhancement attained over one FSR. In fact, both show their peak at the maximum degree of nonreciprocity. However, while  $G_{cav}$  is always null when  $|t_{12}|^2 = 0$ , the TBP is greater than zero (and smaller than 1) because  $\rho_0 \neq 0$ , and decreases with increasing  $|t_{21}|^2$  along the line  $|t_{12}|^2 = 0$ , reaching its minimum at  $|t_{21}|^2 = 1$ .

The benefit of the nonreciprocal coupling in a resonant system shows up more clearly by evaluating the total power enhancement in the nonreciprocal case with respect to the power enhancement achievable in the reciprocal case for the same amount of in-coupled power. This can be illustrated by plotting  $G_{cav}^{NR}/G_{cav}^R$ , where  $G_{cav}^{NR}$  is  $G_{cav}$  for the nonreciprocal system calculated with  $\rho_{in} > \rho_{out}$ , and  $G_{cav}^R$  for the reciprocal one. The results, obtained from the simulations, are plotted in Fig. 6 as a function of the degree of nonreciprocity [with the same conditions of Case (A) in Fig. 3] and compared with the corresponding values of the TBP. Clearly, the ratio  $G_{cav}^{NR}/G_{cav}^R$  increases exponentially with the degree of nonreciprocity, proving that by tailoring the decoupling of  $\rho_{in}$  and  $\rho_{out}$ , the intracavity power can be enhanced much more than what could be done with a reciprocal resonator. We also note that the values of the TBP are in good agreement with those of  $G_{cav}^{NR}/G_{cav}^R$ , meaning that it can be used as a figure of merit to indicate the gain of total power enhancement due to nonreciprocal coupling, with respect to

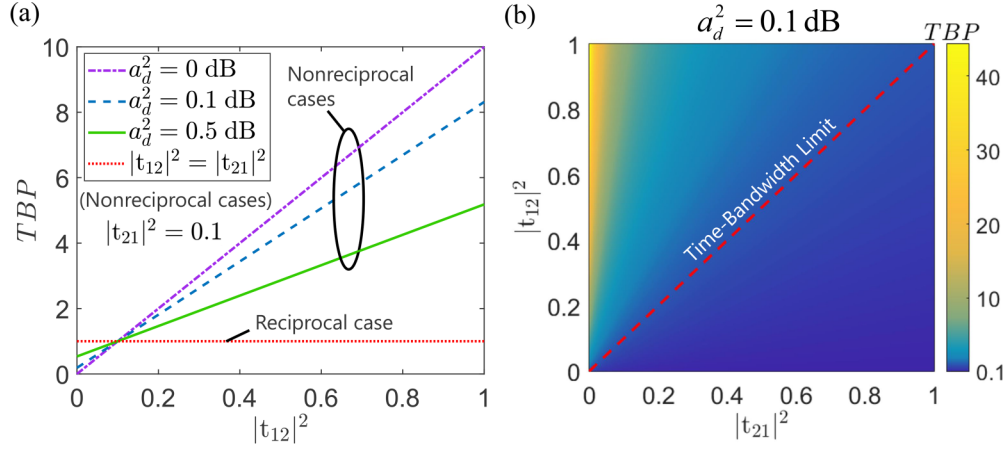


FIG. 5. (a) Comparison between the TBP of a reciprocal and a nonreciprocal resonator plotted as a function of the in-coupling transmittance. The curves of the nonreciprocal cases are relative to resonators with different absorption losses. (b) Graph of the TBP in color scale as a function of the in- and out-coupling transmittance for a resonator with 0.1 dB of internal loss. The red dashed line indicates the values relative to the reciprocal coupling (i.e.,  $TBP = 1$ ), which corresponds to the time-bandwidth limit.

a reciprocal resonator, for an equal amount of in-coupled power.

As a conclusive remark, let us consider the general definition of the TBP ( $TBP = \Delta\omega_{\text{acc}}/\Delta\omega_{\text{cav}}$ ) [43]. It can be rewritten as a ratio between the finesse related to  $\Delta\omega_{\text{cav}}$  and  $\Delta\omega_{\text{acc}}$ , which we name *cavity* and *acceptance Lorentzian finesse*,  $\mathcal{F}_{\text{cav}}$  and  $\mathcal{F}_{\text{acc}}$ , respectively:

$$TBP = \frac{\Delta\omega_{\text{acc}}}{\Delta\omega_{\text{FSR}}} \frac{\Delta\omega_{\text{FSR}}}{\Delta\omega_{\text{cav}}} = \frac{\mathcal{F}_{\text{cav}}}{\mathcal{F}_{\text{acc}}}. \quad (5)$$

The physical meaning of this expression can be found by considering that the cavity finesse calculated using the Lorentzian linewidth represents the number of round trips (times  $2\pi$ ) before the energy stored in the resonator decays to  $1/e$  of its original value [37]. Applying this definition also to the loading process, we can say that the  $\mathcal{F}_{\text{acc}}$  is the number of

round trips the intracavity energy takes to reach its final value, starting from  $1/e$  of this value. Therefore, considering a certain amount of energy stored inside a resonator with  $\rho_{\text{in}} > \rho_{\text{out}}$ , a  $TBP > 1$  implies that the decay time  $\tau_D = 1/\rho_{\text{out}} + 1/\rho_0$  experienced by this energy is longer than that provided by a reciprocal resonator ( $TBP = 1$ ) by an amount equal to the ratio  $\mathcal{F}_{\text{cav}}/\mathcal{F}_{\text{acc}}$ .

#### IV. CONCLUSION

In conclusion, we investigated the implications of the nonreciprocal energy coupling on the TBP and the power balance of a generic resonant cavity. The results obtained by performing an analytical and numerical analysis of the frequency response of the modeled resonant system show that the decoupling of the in- and out-coupling energy rates, as a consequence of the induced nonreciprocity, can significantly improve the power enhancement provided by the resonator compared to the reciprocal case. By evaluating the TBP of such a system, we show that it is greater (smaller) than 1 when  $\rho_{\text{in}} > \rho_{\text{out}}$  ( $\rho_{\text{in}} < \rho_{\text{out}}$ ) and takes its highest value at the maximum degree of nonreciprocity. We provide an interpretation of the TBP as a measure of the increased delay time imparted to a light wave, with respect to what the bandwidth of the resonant structure would allow for the same amount of in-coupled power. This is valid for every finite value of the acceptance and cavity Lorentzian finesse and fits with the time-bandwidth limit ( $\Delta\omega\tau = 1$ ) which, instead, simply links the cavity bandwidth to the photon lifetime, only when the resonator is reciprocal. Moreover, by comparing the total power enhancement in the reciprocal and nonreciprocal case, we proved that the TBP is a figure of merit that characterizes the gain of total power enhancement attained over one FSR through nonreciprocal coupling compared to the reciprocal case, considering the same amount of in-coupled power. Understanding these fundamental relationships for general resonators will allow the development of novel optical devices, using nonreciprocity to further increase field

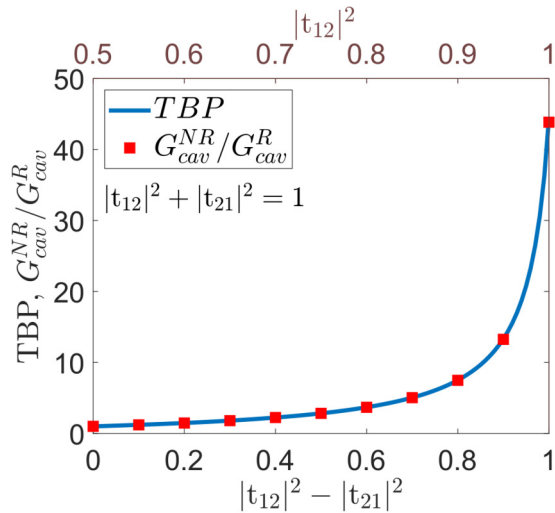


FIG. 6. Comparison between the values of the ratio  $G_{\text{cav}}^{\text{NR}}/G_{\text{cav}}^{\text{R}}$  calculated using the values of  $G_{\text{cav}}$  obtained from the simulations, and the TBP as a function of the degree of nonreciprocity of the system.

enhancements and hence the efficiency of nonlinear optical interactions.

### ACKNOWLEDGMENT

K.L.T. was supported by Hellenic Foundation for Research and Innovation (HFRI), General Secretariat for Research and Technology (GSRT) (Grant No. 1819).

### APPENDIX A: DERIVATION OF EQS. (2) AND (3)

A general expression of the intracavity and reflected spectra of a Gires-Tournois resonator can be derived using the circulating field approach [46]:

$$A = \frac{\mathbf{t}_{12}\sqrt{a_d}}{1 - |\mathbf{r}_{21}|a_d e^{-j\phi_{RT}}} A_{in}, \quad (\text{A1})$$

$$A_R = \left[ \mathbf{r}_{12} + \frac{\mathbf{t}_{12}\mathbf{t}_{21}a_d e^{-j(\phi_{RT}-\phi_{21}^r)}}{1 - |\mathbf{t}_{21}|a_d e^{-j\phi_{RT}}} \right] A_{in}, \quad (\text{A2})$$

where  $a_d = e^{-\alpha_d L_{RT}}$  is the field inner circulation factor that accounts for the nonradiative loss of the resonator,  $A_{in}$  is the amplitude of the input signal, and  $\phi_{RT}$  is the total round-trip phase delay, which is given by the sum of the cavity round-trip phase delay  $\phi_d = \beta(2L_{RT})$  and the phase of  $\mathbf{r}_{21}$  ( $\phi_{21}^r$ ). In these latter expressions,  $L_{RT}$ ,  $\alpha_d$ , and  $\beta$  are the cavity length, the intracavity power attenuation coefficient, and the propagation constant, respectively. Given that  $\phi_{RT} = 2m\pi + \Delta\phi_{RT}$ , where  $\Delta\phi_{RT}$  is the phase detuning from resonance, the exponential term in Eqs. (A1) and (A2) can be written as  $e^{-j\Delta\omega T_{RT}}$ , where  $\Delta\omega = \omega - \omega_0$ , and  $T_{RT} = 2L_{RT}/v_g$  is the cavity round-trip time, with  $v_g$  the group velocity. Also, defining the intrinsic energy decay rate  $\rho_0 = \alpha_d v_g$ , we can rewrite the inner circulation factor in the denominator of Eqs. (A1) and (A2) as  $a_d = e^{-(\rho_0 T_{RT})/2}$ . Using these relations and, recalling that the in- and out-coupling transmittances are related to their corresponding energy rates through  $\rho_{in} = |\mathbf{t}_{12}|^2/T_{RT}$  and  $\rho_{out} = |\mathbf{t}_{21}|^2/T_{RT}$  [37], we can express the intracavity and reflected spectra as a function of  $\rho_{in}$ ,  $\rho_{out}$ ,  $\rho_0$ , and  $\Delta\omega$ :

$$A(\omega) = \frac{\sqrt{\rho_{in} T_{RT}} \sqrt{a_d}}{1 - \exp[\ln(|\mathbf{r}_{21}|) - (\rho_0/2 + j\Delta\omega)T_{RT}]} A_{in}(\omega), \quad (\text{A3})$$

$$A_R(\omega) = \left[ \mathbf{r}_{12} + \frac{\sqrt{\rho_{in}\rho_{out}} T_{RT} a_d \exp[-j(\Delta\omega T_{RT} - \phi_{21}^r)]}{1 - \exp[\ln(|\mathbf{r}_{21}|) - (\rho_0/2 + j\Delta\omega)T_{RT}]} \right] A_{in}(\omega). \quad (\text{A4})$$

### APPENDIX B: DESCRIPTION OF THE SETUP USED FOR THE SIMULATIONS

The Gires-Tournois resonator can be experimentally implemented in the form of a figure-nine cavity, as we have shown in [43], where the nonreciprocal front mirror is realized by the time-modulated Sagnac interferometer. We therefore build the numerical model of the Gires-Tournois resonator using the same layout used in [43]. To be able to explore the full nonreciprocal scenario consisting of an in-coupling

transmittance spanning from 0 to 1, we use a nonreciprocal coupler, instead of a standard directional coupler (see Fig. 7). In fact, as explained in [43], a standard directional coupler can lead, in the presence of phase modulation, only to the maximum in-coupling transmittance ( $|\mathbf{t}_{12}|^2 = 1$ ). Therefore, as we will see, a nonreciprocity of the coupling coefficients of the coupler is required to unlock all the values of the in-coupling transmittance between 0 and 1.

In order to understand how the nonreciprocal coupling is simulated by the time-modulated Sagnac interferometer, we need to examine the equations that govern the wave interference at the coupler [43,61].

Let us consider an optical pulse incident on the R port of the coupler, whose pulse duration is smaller than the cavity round-trip time,  $T_{RT}$ . Specifically, the pulse length is shorter than the distance of the phase modulator from the loop midpoint. This enables the imparting of the phase modulation only to one of the two counterpropagating pulses.

The nonreciprocity of the coupler imposes that the cross and straight coupling coefficients depend on the direction of the light wave. In particular,  $\kappa_a$  and  $\tau_a$  are the cross and straight coupling coefficients, respectively, for the wave propagating from the R or T port toward the inside of the loop, while  $\kappa_b$  and  $\tau_b$  are the cross and straight coupling coefficients respectively for the wave going from inside the loop toward the R or T port. Explicitly, this means that for the left-hand schematic of Fig. 7,  $\kappa_a$  is the coupling efficient from R to 2 and T to 1,  $\tau_a$  is for R to 1 and T to 2,  $\kappa_b$  is for 2 to R and 1 to T, and  $\tau_b$  is for 1 to R and 2 to T. Since the input signal consists of a single pulse, it does not superimpose at the coupler with any other pulse (the same result would be obtained if the input signal was given by a pulse train with a period longer than the cavity RT time and not a multiple of it); the transfer characteristic of the coupler can be described by two distinct scattering matrices, one for each direction of propagation of the wave. We therefore can define  $\mathbf{S}_{Ca}$ , the scattering matrix for the wave propagation toward the inside of the loop, and  $\mathbf{S}_{Cb}$  for the wave coming from within the loop:

$$\mathbf{S}_{Ca} = \begin{bmatrix} \tau_a & -j\kappa_a \\ -j\kappa_a & \tau_a \end{bmatrix}, \quad \mathbf{S}_{Cb} = \begin{bmatrix} \tau_b & -j\kappa_b \\ -j\kappa_b & \tau_b \end{bmatrix}. \quad (\text{B1})$$

A device with such characteristic is included in the VPIPHOTONICS software library as a generic coupler in which it is possible to arbitrarily set the scattering parameters. However, the same behavior can be performed in practice by a time-variant tunable directional coupler made of a four-port Mach-Zehnder interferometer [31].

Passing through the coupler the incoming pulse is split into two pulses whose complex amplitudes can be written as follows:

$$A_{1a} = \tau_a A_{in}, \quad A_{2a} = -j\kappa_a A_{in}, \quad (\text{B2})$$

where  $A_{in}$  is the original complex amplitude of the pulse. If there is no phase modulation the complex amplitudes of the two counterpropagating waves, the clockwise (CW) and counter-clockwise (CCW), are simply

$$A_{cw} = \tau_a A_{in} e^{-j\phi_p}, \quad A_{ccw} = -j\kappa_a A_{in} e^{-j\phi_p}, \quad (\text{B3})$$

where  $\phi_p$  is the phase delay acquired by the optical pulse through the fiber loop. Then, by denoting  $A_T$  and  $A_R$  the

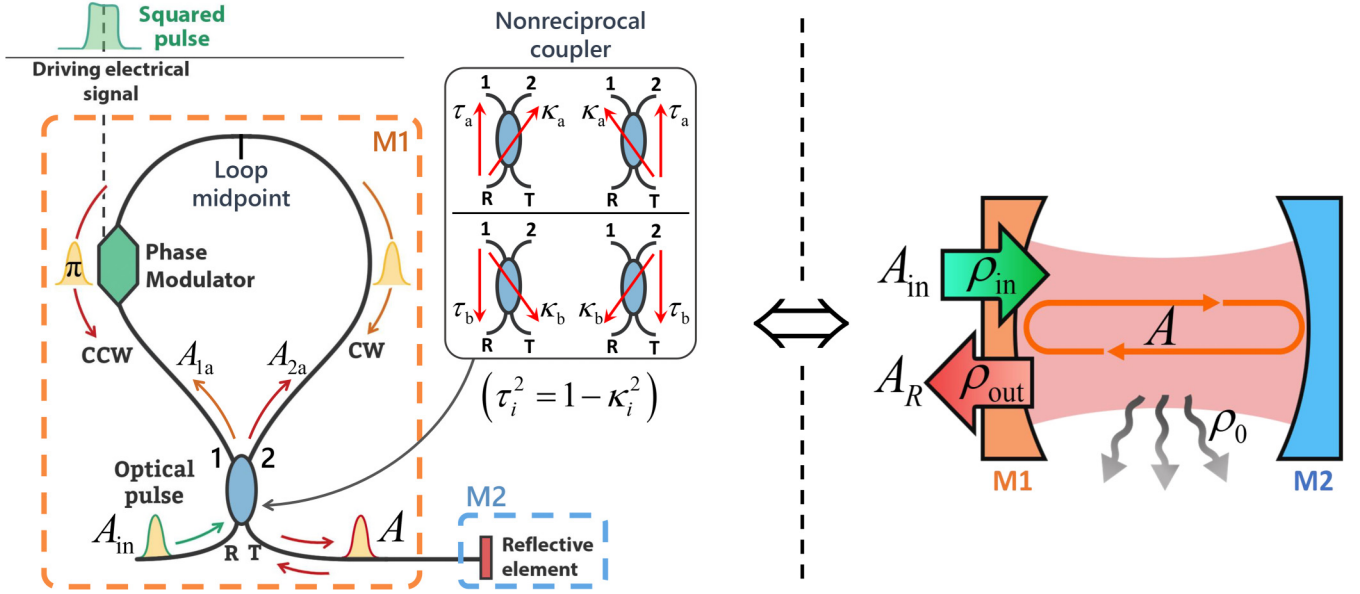


FIG. 7. Schematic representation of the setup used in VPIPHOTONICS for the numerical simulations. The phase modulation in combination with the nonreciprocal coupler both integrated in a Sagnac interferometer ensures a total control of the transmission coefficient of the fiber loop, allowing us to emulate the nonreciprocal front mirror of the Gires-Tournois resonator.

complex amplitudes of the transmitted and reflected portions of the pulse, respectively, the field transmission and reflection coefficients  $\mathbf{t}_0$  and  $\mathbf{r}_0$ , respectively, are easily found:

$$A_T = \tau_b A_{ccw} - j\kappa_b A_{ccw} \Rightarrow \mathbf{t}_0 = \frac{A_T}{A_{in}} = (\tau_a \tau_b - \kappa_a \kappa_b) e^{-j\phi_p}, \quad (\text{B4})$$

$$\begin{aligned} A_R &= -j\kappa_b A_{ccw} + \tau_b A_{ccw} \Rightarrow \mathbf{r}_0 \\ &= \frac{A_R}{A_{in}} = -j(\tau_a \kappa_b + \kappa_a \tau_b) e^{-j\phi_p}, \end{aligned} \quad (\text{B5})$$

where the subscript 0 indicates the absence of the phase modulation.

Conversely, if the phase modulator is electrically gated to shift by  $\pi$  the phase of one of the two counterpropagating

pulses only, say the CCW pulse, the complex amplitude  $A_{ccw}$  in Eq. (B3) becomes

$$A_{ccw} = -j\kappa_a A_{in} e^{-j(\phi_p + \pi)} = j\kappa_a A_{in} e^{-j\phi_p}, \quad (\text{B6})$$

and, therefore, the complex transmission and reflection coefficients,  $\mathbf{t}_\pi$  and  $\mathbf{r}_\pi$ , respectively, exhibited by the Sagnac interferometer will be

$$\mathbf{t}_\pi = (\tau_a \tau_b + \kappa_a \kappa_b) e^{-j\phi_p}, \quad \mathbf{r}_\pi = -j(\tau_a \kappa_b - \kappa_a \tau_b) e^{-j\phi_p}, \quad (\text{B7})$$

where the subscript  $\pi$  indicates the presence of the  $\pi$  phase shift imparted by the phase modulator. In the above expressions, the value of  $\phi_p$  can be arbitrarily set to 0 without loss of generality.

When the electrical signal is applied at the phase modulator at a time  $t_1$ , and for a duration  $t_1 \leq t < t_2$ , the Sagnac

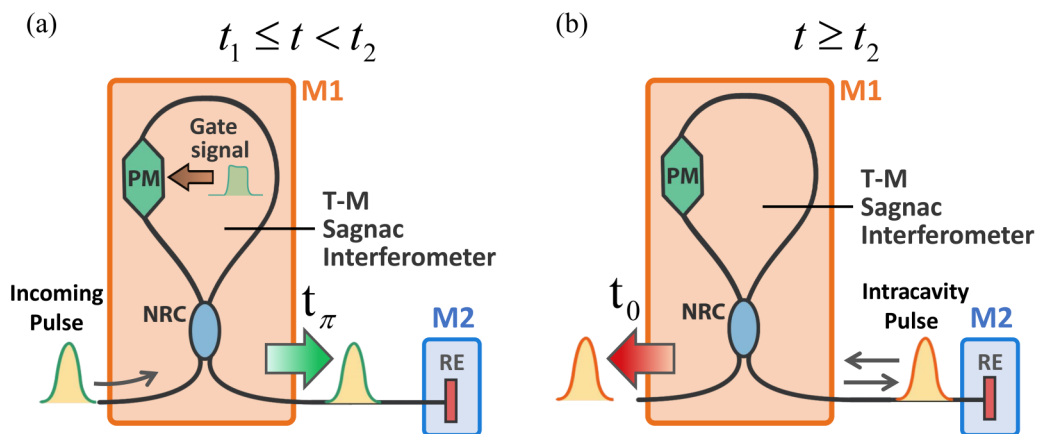


FIG. 8. Schematic representation of the Gires-Tournois resonator in the form of a figure-nine cavity for (a)  $t_1 \leq t < t_2$  and for (b)  $t \geq t_2$ . PM: phase modulator; NRC: nonreciprocal coupler; RE: reflective element.

interferometer exhibits a transmission coefficient  $\mathbf{t}(t_1) = \mathbf{t}_\pi$ , while for the rest of the time ( $t \geq t_2$ ), the transmission coefficient is  $\mathbf{t}(t_2) = \mathbf{t}_0$ . Therefore, the localized time-varying phase modulation, in combination with the nonreciprocal coupler, allows us to arbitrarily vary in time the power transmission coefficient  $\mathbf{t}$  of the Sagnac interferometer. In fact, we can obtain any value of  $\mathbf{t}$  simply by acting on the electrical gating signal and by setting the proper parameters of the scattering matrices of the nonreciprocal coupler. The final result is two effectively different coupling energy rates of the figure-nine resonator, one for  $t_1 \leq t < t_2$  and one for  $t \geq t_2$  which are given, respectively, by

$$\rho(t_1) = \frac{|\mathbf{t}_\pi|^2}{T_{\text{RT}}}, \quad \rho(t_2) = \frac{|\mathbf{t}_0|^2}{T_{\text{RT}}}. \quad (\text{B8})$$

If the incoming optical pulse is synchronized with the electric signal, it is coupled in the resonator through the Sagnac interferometer with a transmission coefficient  $\mathbf{t}_\pi$ , as is depicted in Fig. 8(a). However, while it resonates within the cavity, it is coupled out with a transmission coefficient  $\mathbf{t}_0$  [Fig. 8(b)]. Doing so, although the Sagnac interferometer exhibits a unique transmission coefficient at any given time, the incoming pulse experiences a transmission coefficient that is different from the one experienced by the intracavity pulse ( $\mathbf{t}_\pi \neq \mathbf{t}_0$ ). We can therefore identify  $\mathbf{t}_\pi$  and  $\mathbf{t}_0$  with the transmission coefficients  $\mathbf{t}_{12}$  and  $\mathbf{t}_{21}$ , respectively, and  $\rho(t_1)$  [ $\rho(t_2)$ ] with the in-coupling (out-coupling) energy rate  $\rho_{\text{in}}$  ( $\rho_{\text{out}}$ ) of the Gires-Tournois resonator. Analogously, we identify  $\mathbf{r}_\pi$  and  $\mathbf{r}_0$  with the reflection coefficient  $\mathbf{r}_{12}$  and  $\mathbf{r}_{21}$ , respectively.

In such a system, the acceptance bandwidth corresponds to the bandwidth that the figure-nine resonator exhibits in the time window between  $t_1$  and  $t_2$ , that is,  $\Delta\omega_{\text{acc}} = \rho(t_1) + \rho_0$ , while the cavity bandwidth is the bandwidth that the system exhibits when there is no signal applied to the phase modulator (i.e., for  $t \geq t_2$ ), which is given by  $\Delta\omega_{\text{cav}} = \rho(t_2) + \rho_0$ . Table I shows a summary of the parameters of the VPIPHO-

TABLE I. Table summarizing the correspondences between the parameters of the VPIPHOTONICS simulation figure-nine-based setup and those of the Gires-Tournois resonator model.

VPIPHOTONICS simulation setup	GT resonator model
$\mathbf{t}_\pi = (\tau_a\tau_b + \kappa_a\kappa_b)e^{-j\phi_p}$	$\mathbf{t}_{12}$
$\mathbf{t}_0 = (\tau_a\tau_b - \kappa_a\kappa_b)e^{-j\phi_p}$	$\mathbf{t}_{21}$
$\mathbf{r}_\pi = -j(\tau_a\kappa_b - \kappa_a\tau_b)e^{-j\phi_p}$	$\mathbf{r}_{12}$
$\mathbf{r}_0 = -j(\tau_a\kappa_b + \kappa_a\tau_b)e^{-j\phi_p}$	$\mathbf{r}_{21}$
$\rho(t_1) =  \mathbf{t}_\pi ^2/T_{\text{RT}}$	$\rho_{\text{in}}$
$\rho(t_2) =  \mathbf{t}_0 ^2/T_{\text{RT}}$	$\rho_{\text{out}}$

TONICS simulation setup, based on the figure-nine cavity implementation, and their corresponding parameters of the Gires-Tournois resonator model.

The choice of using a nonreciprocal coupler, instead of a standard directional coupler, can be ultimately clarified by calculating the expressions of  $\mathbf{t}_\pi$  in the case of a directional coupler with cross and straight coupling coefficients,  $\kappa$  and  $\tau$ , respectively. Equation (B7) would then get the following form:

$$\mathbf{t}_\pi = (\tau^2 + \kappa^2)e^{-j\phi_p} = 1, \quad (\text{B9})$$

where we have assumed that the coupler is ideal, i.e.,  $\tau^2 + \kappa^2 = 1$  and that  $\phi_p = 0$ . Therefore, in this case, it would not be possible to obtain an in-coupling transmittance different from 1, thus limiting our parameter space. However, the nonreciprocal coupling is still ensured by the time-variant phase modulation, since  $\mathbf{t}_0$  in this case would be given by

$$\mathbf{t}_0 = (\tau^2 - \kappa^2)e^{-j\phi_p}. \quad (\text{B10})$$

In the case of a 50/50 coupler Eq. (B10) gives  $\mathbf{t}_0 = 0$ , which, together with Eq. (B9), represents the nonreciprocal coupling scenario explored experimentally in [43].

- 
- [1] J. K. Jang, M. Erkintalo, J. Schroder, B. J. Eggleton, S. G. Murdoch, and S. Coen, All-optical buffer based on temporal cavity solitons operating at 10 Gb/s, *Opt. Lett.* **41**, 4526 (2016).
- [2] F. Leo, S. Coen, P. Kockaert, S. P. Gorza, P. Emplit, and M. Haelterman, Temporal cavity solitons in one-dimensional Kerr media as bits in an all-optical buffer, *Nat. Photonics* **4**, 471 (2010).
- [3] M. D. Lukin and A. Imamoglu, Nonlinear Optics and Quantum Entanglement of Ultraslow Photons, *Phys. Rev. Lett.* **84**, 1419 (2000).
- [4] H. Hu, D. Ji, X. Zeng, K. Liu, and Q. Gan, Rainbow trapping in hyperbolic metamaterial waveguide, *Sci. Rep.* **3**, 1249 (2013).
- [5] G. Demésy and S. John, Solar energy trapping with modulated silicon nanowire photonic crystals, *J. Appl. Phys.* **112**, 074326 (2012).
- [6] S. Eyderman, S. John, M. Hafez, S. S. Al-Ameer, T. S. Al-Harby, Y. Al-Hadeethi, and D. M. Bouwes, Light-trapping optimization in wet-etched silicon photonic crystal solar cells, *J. Appl. Phys.* **118**, 023103 (2015).
- [7] S. Eyderman and S. John, Light-trapping and recycling for extraordinary power conversion in ultra-thin gallium-arsenide solar cells, *Sci. Rep.* **6**, 28303 (2016).
- [8] J. B. Khurgin, Slow light in various media: A tutorial, *Adv. Opt. Photonics* **2**, 287 (2010).
- [9] T. Baba, Slow light in photonic crystals, *Nat. Photonics* **2**, 465 (2008).
- [10] M. González-Herráez, K.-Y. Song, and L. Thévenaz, Optically controlled slow and fast light in optical fibers using stimulated Brillouin scattering, *Appl. Phys. Lett.* **87**, 081113 (2005).
- [11] S. A. Schulz, L. O’Faolain, D. M. Beggs, T. P. White, A. Melloni, and T. F. Krauss, Dispersion engineered slow light in photonic crystals: A comparison, *J. Opt.* **12**, 104004 (2010).
- [12] L. Thévenaz, Slow and fast light in optical fibres, *Nat. Photonics* **2**, 474 (2008).
- [13] T. F. Krauss, Why do we need slow light? *Nat. Photonics* **2**, 448 (2008).
- [14] S. John, Why trap light? *Nat. Mater.* **11**, 997 (2012).
- [15] K. L. Tsakmakidis, O. Hess, R. W. Boyd, and X. Zhang, Ultra-slow waves on the nanoscale, *Science* **358**, eaan5196 (2017).

- [16] C. W. Hsu, B. Zhen, J. Lee, S. L. Chua, S. G. Johnson, J. D. Joannopoulos, and M. Soljačić, Observation of trapped light within the radiation continuum, *Nature* **499**, 188 (2013).
- [17] T. Tanabe, M. Notomi, H. Taniyama, and E. Kuramochi, Dynamic Release of Trapped Light from an Ultrahigh- $Q$  Nanocavity via Adiabatic Frequency Tuning, *Phys. Rev. Lett.* **102**, 043907 (2009).
- [18] J. Upham, Y. Fujita, Y. Kawamoto, Y. Tanaka, B. S. Song, T. Asano, and S. Noda, The capture, hold and forward release of an optical pulse from a dynamic photonic crystal nanocavity, *Opt. Express* **21**, 3809 (2013).
- [19] K. L. Tsakmakidis, A. D. Boardman, and O. Hess, “Trapped rainbow” storage of light in metamaterials, *Nature* **450**, 397 (2007).
- [20] M. F. Yanik and S. Fan, Stopping Light All Optically, *Phys. Rev. Lett.* **92**, 083901 (2004).
- [21] M. F. Yanik and S. Fan, Stopping and storing light coherently, *Phys. Rev. A* **71**, 013803 (2005).
- [22] H. J. S. Dorren, M. T. Hill, Y. Liu, N. Calabretta, A. Srivatsa, F. M. Huijskens, H. de Waardt, and G. D. Khoe, Optical packet switching and buffering by using all-optical signal processing methods, *J. Light. Technol.* **21**, 2 (2003).
- [23] A. E. Willner, S. Khaleghi, M. R. Chitgarha, and O. F. Yilmaz, All-optical signal processing, *J. Light. Technol.* **32**, 660 (2014).
- [24] Y. Okawachi, M. S. Bigelow, J. E. Sharping, Z. Zhu, A. Schweinsberg, D. J. Gauthier, R. W. Boyd, and A. L. Gaeta, Tunable All-Optical Delays via Brillouin Slow Light in an Optical Fiber, *Phys. Rev. Lett.* **94**, 153902 (2005).
- [25] Q. Gan, Z. Fu, Y. J. Ding, and F. J. Bartoli, Ultrawide-Bandwidth Slow-Light System based on THz Plasmonic Graded Metallic Grating Structures, *Phys. Rev. Lett.* **100**, 256803 (2008).
- [26] J. Cardenas, M. A. Foster, N. Sherwood-Droz, C. B. Poitras, H. L. R. Lira, B. Yhang, A. L. Gaeta, J. B. Khurgin, P. Morton, and M. Lipson, Wide-bandwidth continuously tunable optical delay line using silicon microring resonators, *Opt. Express* **18**, 26525 (2010).
- [27] F. Xia, L. Sekaric, and Y. Vlasov, Ultracompact optical buffers on a silicon chip, *Nat. Photonics* **1**, 65 (2007).
- [28] L. Maleki, A. B. Matsko, A. A. Savchenkov, and V. S. Ilchenko, Tunable delay line with interacting whispering-gallery-mode resonators, *Opt. Lett.* **29**, 626 (2004).
- [29] J. B. Khurgin and P. A. Morton, Tunable wideband optical delay line based on balanced coupled resonator structures, *Opt. Lett.* **34**, 2655 (2009).
- [30] W. Yoshiki, Y. Honda, T. Tetsumoto, K. Furusawa, N. Sekine, and T. Tanabe, All-optical tunable buffering with coupled ultrahigh  $Q$  whispering gallery mode microcavities, *Sci. Rep.* **7**, 10688 (2017).
- [31] W. V. Sorin and R. S. Tucker, Optical pulse storage, shaping, and wavelength conversion in resonators with controllable input coupling, *J. Light. Technol.* **27**, 2587 (2009).
- [32] T. J. Kippenberg, R. Holzwarth, and S. A. Diddams, Microresonator-based optical frequency combs, *Science* **332**, 555 (2011).
- [33] T. J. Kippenberg, A. L. Gaeta, M. Lipson, and M. L. Gorodetsky, Dissipative Kerr solitons in optical microresonators, *Science* **361**, eaan8083 (2018).
- [34] R. S. Tucker, P.-C. Ku, and C. J. Chang-Hasnain, Slow-Light Optical Buffers: Capabilities and Fundamental Limitations, *J. Light. Technol.* **23**, 4046 (2005).
- [35] R. W. Boyd, D. J. Gauthier, A. L. Gaeta, and A. E. Willner, Maximum time delay achievable on propagation through a slow-light medium, *Phys. Rev. A* **71**, 023801 (2005).
- [36] J. B. Khurgin, Performance limits of delay lines based on optical amplifiers, *Opt. Lett.* **31**, 948 (2006).
- [37] V. Van, *Optical Microring Resonators: Theory, Techniques, and Applications* (CRC Press, Boca Raton, FL, 2017), pp. 35, 54, 75.
- [38] R. S. Quimby, *Photonics and Lasers: An Introduction* (John Wiley & Sons, New York, 2006), p. 298.
- [39] W. Demtröder, *Laser Spectroscopy I* (Springer, Berlin, 2014), Vol. 1, p. 79.
- [40] J. B. Khurgin, Dispersion and loss limitation on the performance of optical delay lines based on coupled resonant structures, *Opt. Lett.* **32**, 133 (2007).
- [41] D. A. B. Miller, Fundamental Limit to Linear One-Dimensional Slow Light Structures, *Phys. Rev. Lett.* **99**, 203903 (2007).
- [42] K. L. Tsakmakidis, L. Shen, S. A. Schulz, X. Zheng, J. Upham, X. Deng, H. Altug, A. F. Vakakis, and R. W. Boyd, Breaking Lorentz reciprocity to overcome the time-bandwidth limit in physics and engineering, *Science* **356**, 1260 (2017).
- [43] I. Cardea, D. Grassani, S. J. Fabbri, J. Upham, R. W. Boyd, H. Altug, S. A. Schulz, K. L. Tsakmakidis, and C. S. Brès, Arbitrarily high time bandwidth performance in a nonreciprocal optical resonator with broken time invariance, *Sci. Rep.* **10**, 15752 (2020).
- [44] D. L. Sounas and A. Alù, Non-reciprocal photonics based on time modulation, *Nat. Photonics* **11**, 774 (2017).
- [45] F. Gires and P. Tournois, Interféromètre utilisable pour la compression d’impulsions lumineuses modulées en fréquence, *C. R. Acad. Sci. Paris* **258**, 6112 (1964).
- [46] A. Yariv and P. Yeh, *Photonics: Optical Electronics in Modern Communications*, 6th ed. (Oxford University Press, Oxford, 2006), pp. 160, 168.
- [47] C. Caloz, A. Alù, S. Tretyakov, D. Sounas, K. Achouri, and Z. L. Deck-Léger, Electromagnetic Nonreciprocity, *Phys. Rev. Appl.* **10**, 047001 (2018).
- [48] S. A. Mann, D. L. Sounas, and A. Alù, Nonreciprocal cavities and the time-bandwidth limit, *Optica* **6**, 104 (2019).
- [49] K. Tsakmakidis, Y. You, T. Stefański, and L. Shen, Nonreciprocal cavities and the time-bandwidth limit: Comment, *Optica* **7**, 1097 (2020).
- [50] A. Alu, S. Mann, and D. Sounas, Nonreciprocal cavities and the time-bandwidth limit: Reply, *Optica* **7**, 1102 (2020).
- [51] V. Asadchy, M. S. Mirmoosa, A. Díaz-Rubio, S. Fan, and S. A. Tretyakov, Tutorial on electromagnetic nonreciprocity and its origins, *Proc. IEEE* **108**, 1684 (2020).
- [52] A. Yariv, Universal relations for coupling of optical power between microresonators and dielectric waveguides, *Electron. Lett.* **36**, 321 (2000).
- [53] H. A. Haus, *Waves and Fields in Optoelectronics* (Prentice-Hall, Upper Saddle River, NJ, 1984), pp. 197, 228.
- [54] S. Fan, W. Suh, and J. D. Joannopoulos, Temporal coupled-mode theory for the Fano resonance in optical resonators, *J. Opt. Soc. Am. A* **20**, 569 (2003).

- [55] Z. Wang, S. Fan, and W. Suh, Temporal coupled-mode theory and the presence of non-orthogonal modes in lossless multimode cavities, *IEEE J. Quantum Electron.* **40**, 1511 (2004).
- [56] J. D. Joannopoulos, S. G. Johnson, J. N. Winn, and R. D. Meade, *Photonic Crystals: Molding the Flow of Light*, 2nd ed. (Princeton University Press, Princeton, NJ, 2008), pp. 197–203.
- [57] Z. Zhao, C. Guo, and S. Fan, Connection of temporal coupled-mode-theory formalisms for a resonant optical system and its time-reversal conjugate, *Phys. Rev. A* **99**, 033839 (2019).
- [58] K. X. Wang, Time-reversal symmetry in temporal coupled-mode theory and nonreciprocal device applications, *Opt. Lett.* **43**, 5623 (2018).
- [59] N. Ismail, C. C. Kores, D. Geskus, and M. Pollnau, Fabry-Pérot resonator: Spectral line shapes, generic and related Airy distributions, linewidths, finesse, and performance at low or frequency-dependent reflectivity, *Opt. Express* **24**, 16366 (2016).
- [60] <https://www.vpiphotonics.com>.
- [61] D. B. Mortimore, Fiber loop reflectors, *J. Light. Technol.* **6**, 1217 (1988).